Front. Struct. Civ. Eng. 2025, 19(5): 681–698
https://doi.org/10.1007/s11709-025-1163-x

RESEARCH ARTICLE

Experimental study on seismic behavior of L-shaped-section steel reinforced high-strength concrete shear walls for core tube of super-tall buildings

Qiang ZHANG[a], Bin ZHAO[a*], Linyuan MA[a], Xilin Lu[a], Xiangyong NI[b], Kun DING[c], Jianlong ZHOU[d]

[a] *State Key Laboratory of Disaster Reduction in Civil Engineering, Tongji University, Shanghai 200092, China*
[b] *Department of Civil Engineering, Shanghai University, Shanghai 200444, China*
[c] *Shanghai Industrial Investment North Bund New Landmark Construction and Development Co., Ltd., Shanghai 200000, China*
[d] *East China Architectural Design & Research Institute Co., Ltd., Shanghai 200011, China*
[*] *Corresponding author. E-mail: binzh@tongji.edu.cn*

© Higher Education Press 2025

ABSTRACT High-strength concrete and shape steel are combined to form composite shear wall members to address the cross-section oversize of core tube shear walls at the bottom of tall and super-tall buildings. However, the existing investigation focus on rectangular shear walls, and insufficient study has been conducted on L-shaped shear walls. To better understand the seismic performance of L-shaped-section steel reinforced high-strength concrete ($f_{cu} \geqslant 60$ MPa) shear walls (LSRHCW), four such specimens with distinct dimensions, reinforcement ratios and concrete strengths were tested under cyclic loading and high axial compression ratio ($n = 0.5$), and the lateral cyclic loading direction makes an angle of 45° with the wall limb length direction. The influence of improving concrete strength and reducing the steel and reinforcement ratios on the seismic performance is investigated. The results show that under high axial compression ratio, the specimens fail in flexure-shear mode due to strength reduction caused by concrete crushing, and exhibit excellent deformation performance (maximum drift ratio capacity, 3.03%). The wall specimens built with different strength concrete and shape steel ratios demonstrate comparable strength, deformation and initial stiffness. This suggests that the reinforcement ratio of LSRHCWs can be effectively reduced by upgrading concrete strength, while still maintaining their seismic performance.

KEYWORDS L-shaped-section steel reinforced high-strength concrete shear walls, loading direction, seismic performance, cyclic loading test, high axial compression ratio

1 Introduction

Shear walls have shown excellent seismic performance in many large earthquakes, and they are often applied as the main lateral support system of tall and super-tall buildings. However, due to the immense vertical load, shear wall members at the bottom of these buildings often require a thick wall to meet the demand of the deformation and axial compression ratio, while it may lead to the increase of structural cost and seismic effect, and decrease of building usable area. With the development of civil engineering, the performance requirements of building structures on materials have become higher and higher, and many high-performance materials have emerged, playing a huge role in improving structural performance and reducing material consumption. High-strength concrete (HSC), a common and mature high-performance material, has been extensively used in practical projects. It provides a technical approach to address the challenge of excessive thickness in bottom shear wall members. Although HSC has various advantages, such as high compressive strength and elasticity modulus, its brittleness has also increased, leading to a need to improve its ductility for wider application. To overcome this issue, researchers have proposed various types of HSC shear walls,

Article history: Received Jun 5, 2024; Accepted Dec 12, 2024

including steel-reinforced HSC walls [1,2], high-strength (HS) stirrup-confined shear walls [3,4], steel tube shear walls [5], steel fiber-reinforced shear walls [6], steel plate concrete walls [7] and built-in truss shear walls [8]. Among them, shape steel-reinforced HSC walls are commonly used in earthquake-prone tall buildings because of their advantages of high bearing capacity, large stiffness, small size, good ductility, ease of construction, and short construction period [9].

In practical engineering application, most shear walls adopt non-rectangular cross-sections, such as "I", "L", "[" and "T"-shaped cross-sections. The interaction between the flange and web of this type of shear wall results in mechanical performance that deviates significantly from that of a standard rectangular shear wall, making it a big challenge to apply existing research on non-rectangular shear walls. However, current research on flanged shear walls is limited, and research on shape steel reinforced HSC shear walls with flanges is even less developed. L-shaped shear wall members are often used in building structure corners, elevator shaft structures, etc., which are very important to the overall safety performance of the structure. This paper aims to better understand the seismic performance of L-shaped-section steel reinforced high-strength concrete shear walls (LSRHCW).

Existing research has demonstrated that the failure mode of high steel-reinforced concrete (SRC) walls is mainly controlled by flexure, while the failure mode of low SRC walls is mainly controlled by shearing. Middle-high SRC walls experience both flexure and shear failure modes. Cyclic loading tests of high SRC walls have shown that the failure of the walls is caused by the concrete crushing at the toes, and the hysteretic curves are full, indicating good energy dissipation performance. However, bond-slip failure between steel and concrete and compression buckling of steel in the late loading period reduce the strength of the walls [10]. Setting shape steel in the boundary constraints of the wall can effectively enhance the bearing capacity and stiffness of the specimen, as well as the deformation and energy dissipation performance [11–12]. Enhancing the steel ratio of the wall boundary constraints can also helpful to improve the deformation and energy dissipation performance of the specimens [13]. By increasing the axial compression ratio, the strength and stiffness of steel-reinforced ordinary concrete shear walls can be improved, but deformation capacity of the wall are reduced [14–17]. Low-rise SRC shear walls exhibit obvious pinching of hysteretic curves, but insufficient deformation and energy dissipation performance. Setting a rigid frame in the low SRC shear wall can be an effective second seismic defense line, so as to enhance its seismic performance [18–19]. Middle-high SRC shear walls show a flexural-shear failure mode, which is influenced by the shear-span, axial compression, steel ratio, and web reinforcement ratios [20–22]. Deformation and energy dissipation performance of medium-high SRC shear walls is between high and low walls. The form of shape steel has little influence on the performance of SRC walls under earthquake action [23–25]. In addition, experiments on T-shaped SRC shear walls show that the bearing capacity, stiffness, and energy consumption are larger, and the pinching effect is smaller, when the flange is in tension [26]. The above research shows that shape steel has effectively improved the seismic performance of normal walls, so some scholars try to apply shape steel in HSC shear walls. Dan et al. [27] experimentally investigated the behavior of shape steel reinforced C60 HSC shear walls under cyclic loading. This type of wall has outstanding energy dissipation capacity, and the HSC at the toes crushed before the shape steel yielded, and the steel in elastic state ensures the ductility of the wall after concrete crushing. Bai et al. [28] carried out cyclic loading tests on eight middle-rise shape steel reinforced HSC walls. The failure mode of the wall specimens was controlled by flexure, and the failure was caused by the strength reduction owing to the crushing of HSC at the toes of the wall. The hysteretic curves of each specimen are well full, showing good energy dissipation capacity and slight pinching phenomenon.

To increase the out-of-plane stiffness of shear wall members, the shear wall members are generally designed to be with flanged sections. In recent years, the scholars have conducted extensive research on the seismic performance of shear walls with flanges. Hoult et al. [29] conducted different cyclic loading tests on U-shaped shear walls. The lateral reverse-cyclic bending test about the minor axis showed that the failure of U-shaped shear walls was owing to the external instability of flange surface induced by the crushing of flange concrete and the buckling of steel bars, and the reverse-cyclic rotation test showed that the wall exhibited an out-of-plane diagonal compression failure of one flange caused by a combination of transversal shear and flexure. Moreover, Hoult [30] used a 3D finite element softer ware VecTor3 to study the shear lag effect of RC U-shaped walls under shear force. Menegon et al. [31] conducted an experimental study on the lateral drift behavior of precast box-shaped building core wall specimens under cyclic loading, and grout tube connections were utilized for the joints of the precast walls. The results showed that the precast building core wall specimens were approximately 25% more flexible than an equivalent cast in situ version. Ma et al. [32], Eom et al. [33], Zhang and Li [34], Lan et al. [35] studied the influence of axial compression ratio on the seismic performance of T-shaped shear walls based on pseudo-static tests. The research shows that the axial compression ratio can improve the bearing capacity of T-shaped shear walls, but reduce their ductility, which is similar to the characteristics of rectangular shear walls.

Lim et al. [36] assembled the rectangular shear wall members into a T-shaped shear wall by means of the door-valve connectors, and conducted a cyclic loading test. The study showed that this type of shear wall exhibited reasonable stiffness, strength, ductility and energy dissipation characteristics, and its failure characteristics included welding failure of the C-shaped connector and concrete crushing at the free end of the web plate. Karamlou and Kabir [37], Chaouch et al. [38], Kabir et al. [39] investigated the seismic performance of L-shaped walls, and the results show that when the L-shaped wall is loaded along the length of the limb, the wall is destroyed by the concrete at the free end of the web, and the bearing capacity of the shear wall is higher when the flange is in tension.

Although scholars at home and abroad have done a lot of research on SFC shear walls and got some results, there are still the following aspects in the research that need to be improved.

1) Most of the existing research is aimed at steel and ordinary concrete shear walls, and there is less research on steel high-strength concrete (SHSC) shear walls.

2) The existing research on SRC shear walls focuses on rectangular shear walls. The research on SRC shear walls with flanges is relatively lagging.

3) At present, there is less research on SHSC shear walls under high axial compression ratio. Especially, the seismic performance of this kind of shear walls under the limit value of axial compression ratio has not been reported.

4) Under the action of earthquakes and wind, the direction of the lateral load that the L-shaped shear wall bears is uncertain. But in the existing research, the lateral cyclic load loading direction of the L-shaped shear wall is mostly the length direction of the wall limb, and there is less research on the seismic performance of the L-shaped shear wall in other loading directions.

It is great to see that researchers are continuing to explore new areas of study and work toward addressing the existing research gaps in steel reinforced HSC walls. The deficiencies mentioned, such as the lack of research on steel reinforced HSC shear walls with L-shaped cross-section under different loading directions, indicate a need for further exploration in these areas. The proposed experimental study on the seismic performance of LSRHCWs under high axial compression ratio is a step toward filling these gaps. By testing four specimens under cyclic loading and exploring the seismic performance of the wall under different sizes, steel ratios, and concrete strengths, researchers can gain valuable insights into how to improve the seismic performance of these walls while saving cost. Overall, this research can contribute to the development of more effective and reliable steel reinforced HSC walls, which can ultimately improve the safety and resilience of infrastructure in earthquake-prone areas.

2 Specimen design

2.1 Design details

The test aims to study the feasibility of using shape steel to strength the seismic performance of HSC shear walls, and reducing the shape steel and reinforcing bar ratios by improving the concrete strength, while ensuring the seismic performance of LSRHCWs. Since the section size of shear wall in high-rise buildings decreases with the rise of height and L-shaped form is often used at the corner of walls, two kinds of L-shaped shear walls with different section sizes were set.

According to the prototypes of the actual walls, four LSRHCW specimens with a 1/6 scale were designed. Two practical shear wall members with different sizes were selected used as the prototypes for the 1/6 scaled wall specimens, the comparison of scaled and prototype walls are summarized in Table 1. The building prototype is the Zhongnan Center, which is located in the core CBD area of Suzhou Jinji Lake. The total construction area of the project is about 50000 m^2, 103 floors above ground, 6 floors underground, and the cornice height is 499 m, making it the tallest building under construction in Suzhou, as presented in Fig. 1. The bottom shear wall members of the Zhongnan Center were selected as the prototypes.

The scaled wall specimens use the same concrete material with and the prototype walls, and the reinforcement structures and reinforcement ratios are exactly the same. The four wall specimens were respectively named C60-L, C80-L, C60-S, and C80-S, where C60 and C80 represent concrete strengths used in the wall specimens, and L and S represented larger and

Table 1 Scaled wall specimen design

Specimen	Prototype wall			Scaled wall specimen		
	Length (mm)	Thickness (mm)	Height (mm)	Length (mm)	Thickness (mm)	Height (mm)
C60-L	4000	1000	12000	664	166	2000
C80-L	4000	1000	12000	664	166	2000
C60-S	3600	900	10800	600	150	1800
C80-S	3600	900	10800	600	150	1800



(a)

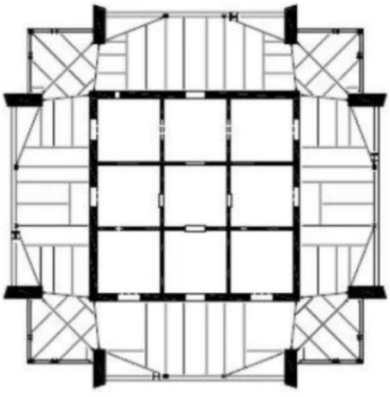

(b)

Fig. 1 Elevation and plan graphs of Zhongnan Center: (a) elevation graph of Zhongnan Center; (b) plane graph.

smaller dimensions, respectively. The design of equal strength was adopted for Specimens C60/C80-L and C60/C80-S, which means that the design strength of Specimens C60/C80-L is the same, as well as Specimens C60/C80-S. The cross-section reinforcement of C60/C80-L and C60/C80-S was presented in Figs. 2(a) and 2(b), respectively. Four rows of vertical and horizontal distribution bars were arranged in total, with a ratio of distribution steel bars of 0.50%, which is the same with the prototype walls, and meets the minimum requirement of 0.25% in the code [40]. The details of the wall specimens are summarized in Table 2.

According to the JGJ3-2010 [40], LSRHCW specimens were designed with three boundary constraints set at the free ends of the two wall limbs and the corner of the two limbs, shown as Fig. 2. The boundary constraints all meet the design requirements of JGJ3-2010 [40]. One shape steel was arranged in each boundary constraint of the wall, and the size of the shape steel of the wall specimens is shown in Table 3.

The axial compression ratio, n, is the ratio of the axial compression load to the product of concrete strength and cross-section area, and it indicates the ratio of the external load to its vertical carrying capacity, which can be obtained by Eq. (1). The weight of the concrete wall plus the upper loading beam is about 85.1 kN, accounting for about 2.1% of the axial load, and converted axial compression ratio is about 0.0011, so its influence on the axial compression ratio is ignored when calculating the axial compression ratio.

$$n = \frac{N}{f_{ck}A}, \tag{1}$$

where A is the cross-section area of the wall specimens, and f_{ck} is axial concrete strength. The f_{ck} values of C60 and C80 are 38.5 and 50.2 MPa, respectively [41].

I-shape steel with the yield strength grade of Q345 (nominal yield strength is 345 MPa) was chosen as for the reinforcement, and the details of shape steel used in each wall are listed in Table 3. To enhance the bond strength between the shape steel and HSC, shear studs were arranged on the flanges of I-shape steel. According to the prototype walls, two rows of shear studs were welded at the two flanges, and the pacing along the length direction of shape steel was 70 mm.

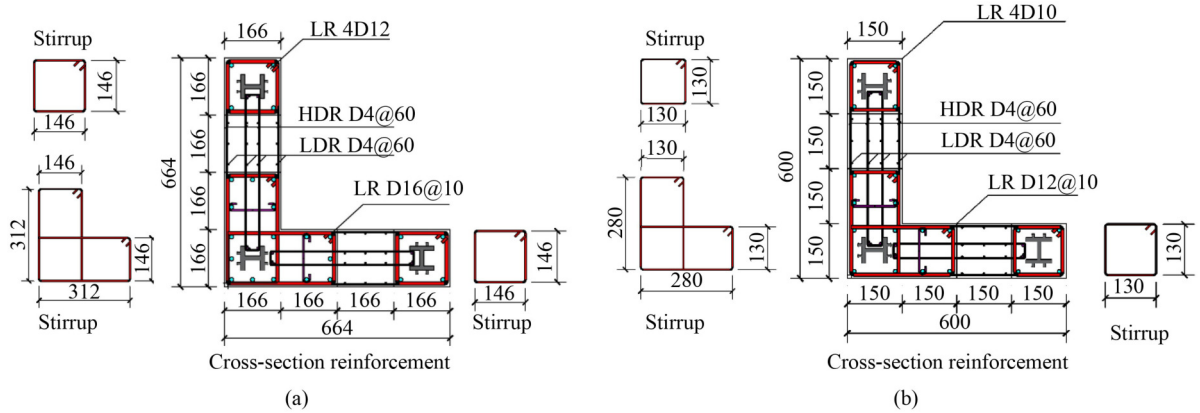

Fig. 2 Reinforcement design of shear wall specimens: (a) specimens C60/C80-L; (b) specimens C60/C80-S. (Note: LR is longitudinal reinforcement, HDR is horizontal distribution reinforcement, LDR is longitudinal distribution reinforcement.)

Table 2 Specimen design details

Specimen	Concrete grade	Model size (mm) (Length × thickness × height)	Free end		Corner		n	N (kN)
			ρ_{l1} (%)	ρ_{s1} (%)	ρ_{l2} (%)	ρ_{s2} (%)		
C60-L	C60	664 × 166 × 2000	1.64	8.1	1.52	2.70	0.5	3684
C80-L	C80	664 × 166 × 2000	1.64	3.63	1.52	1.21		3960
C60-S	C60	600 × 150 × 1800	1.4	8.1	1.4	2.70		2958
C80-S	C80	600 × 150 × 1800	1.4	3.11	1.4	1.04		3081

Note: ρ_{l1} is longitudinal reinforcement ratio in free end, ρ_{s1} is shape steel ratio in free end, ρ_{l2} is longitudinal reinforcement ratio in corner, ρ_{s2} is shape steel ratio in corner, n is axial load ratio, and N is axial constant load force.

Table 3 Shape steel details

Specimen	Height (mm)	Width (mm)	Web (mm)	Flange (mm)
C60-L	70	70	12	12
C80-L	70	70	5	5
C60-S	70	70	8	10
C80-S	70	40	5	5

2.2 Material performance

Two types of HSC (C60 vs. C80) were used in the wall specimens, and each wall specimen was poured at one time. Additionally, six concrete cubes (side length of 150 mm) were reserved for each HSC [42], which were used to measure the cubic compressive strength (f_{cu}) by universal testing machine, shown as Fig. 3(a), and the results are listed in Table 4. The elastic modulus of two kinds of concrete according to the empirical formula of concrete design code GB 50010-2010 [41], as shown below:

$$E_c = \frac{10^5}{2.2 + \frac{34.7}{f_{cu}}} (\text{MPa}). \tag{2}$$

Regarding the mechanical properties of steel bars, the information provided states that the values meet the requirement of GB/T 228.1-2010 [43], and the test setup is shown as Fig. 3(b), and the mechanical details are summarized in Table 3. Moreover, shaped steel samples were prepared and tested according to GB/T 228.1-2010 [43], and they are tested by the universal test machine (shown as Fig. 3(c)) to obtain the yield and tensile strength of shaped steel with different thickness, where the results are summarized in Table 4.

Regarding the mechanical properties of steel bars, the information provided states that the values meet the requirement of GB/T 228.1-2010 [43], and the mechanical details are summarized in Table 5. Moreover, shape steel samples were prepared and tested according to GB/T 228.1-2010 [43], and the yield and tensile strength of shape steel with different thickness is summarized in Table 6.

2.3 Loading test setup and measuring scheme

The test setup is a cantilever beam loading system, shown as Fig. 4, where each shear wall specimen is loaded to a lateral cyclic load and constant axial compressive load. The loading setup of the test is built according to Chinese seismic test code of JGJ/T 101-2015 [44], aiming to simulate the real force and deformation state of shear wall members in earthquake. The bottom beam of the wall specimen is connected to the laboratory foundation through the reserved holes using the HS bolts, and the purpose is to simulate the boundary conditions of the wall bottom connected to the foundation. The vertical

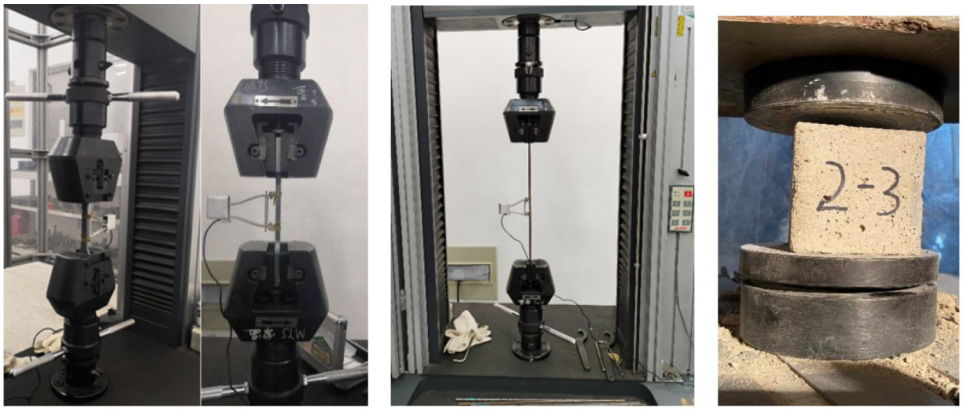

(a) (b) (c)

Fig. 3 Material test setup: (a) tensile test of steel plate; (b) tensile test of reinforcing bars; (c) compression test of concrete cube.

Table 4 Concrete strength

Concrete grade	f_{cu} (MPa)	Mean (MPa)	E_c (MPa)
C60	62.9	60.8	3.61×10^4
	65.3		
	54.2		
C80	77.1	86.7	3.85×10^4
	96.4		
	86.7		

Table 5 Test results of HRB400 steel bars

Diameter (mm)	E_s (MPa)	Yield strength (MPa)	Tensile strength (MPa)	Elongation (%)
4	2.12×10^5	477	546	18.3
6	1.95×10^5	500	592	20.3
8	2.01×10^5	480	599	19.3
10	2.04×10^5	473	553	25.5
14	1.99×10^5	424	625	28.3

Table 6 Mechanical property of shape steel

Thickness (mm)	E_s (MPa)	Yield strength (MPa)	Tensile strength (MPa)
5	2.08×10^5	412	536
8	2.04×10^5	460	597
10	2.01×10^5	483	621
12	1.95×10^5	495	645

hydraulic jack applies the axial load to the upper loading beam on the wall specimens through the steel frame, which keeps constant during the loading process, and is used to simulate the vertical load handed down by the superstructure on the wall. When the vertical load is applied to the design value, the lateral cyclic load is applied through the horizontal actuator to simulate the force state of the wall members during the earthquake. The hydraulic servo actuator is connected to the strong wall in the laboratory for loading the lateral cyclic force. Hydraulic jack is used to apply the vertical load through the strong steel frame, and the axial compressive load keeps constant throughout the loading process.

During the laboratory test, the axial load is first applied to the design values and keeps constant during the whole test process. Subsequently, applying the lateral cyclic loading based on the loading procedure presented in Fig. 5(a), and the positive and negative loading directions are shown as Fig. 5(b). Each loading target circulates for three times until the specimen fails. When any of the following phenomena occur in the wall specimen, it is considered to be in a state of failure: 1) the lateral load decreases to 85% of the previous maximum force; 2) cannot bear axial load; 3) reinforcement bar fracture.

All shear wall specimens are loaded horizontally at the angle of 45° to the wall limb length direction. The cyclic loading is controlled by the top displacement, with the loading program divided into two stages. For the elastic stage, the loading displacement is increased by 1 mm at each stage, and each stage is cycled separately. Once the yield stage reaches, differential reciprocating loading is carried out and each stage is circulated for three times. The yield displacement is selected based on the displacement load at which the first tensile reinforcing bar yields. The test loading is intended to obtain the deformation state of the wall specimen corresponding to the lateral shear force of small earthquake, moderate earthquake, and large earthquake. During the laboratory test, the continuity and uniformity of cyclic loading

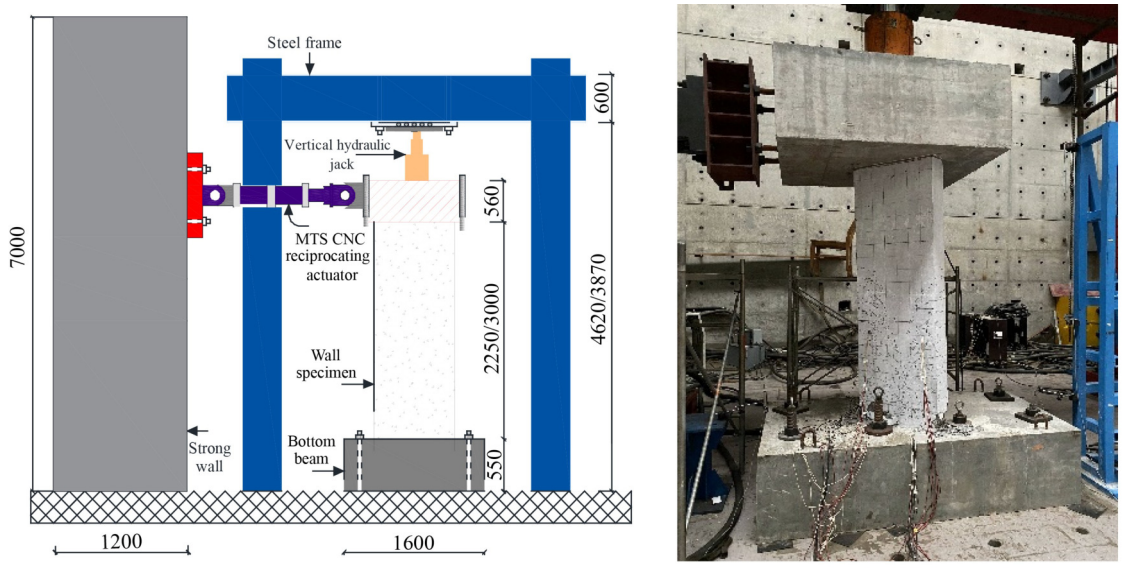

(a) (b)

Fig. 4 Test loading setup (unit: mm): (a) schematic drawing; (b) lab test setup.

should be maintained, and the loading and unloading speeds remain consistent, as depicted in Fig. 4.

2.4 Measuring device

During the entire loading process, the strain gauges (SG) are utilized to monitor the strain variation of the steel bars and shape steel. The SG placement is depicted in Figs. 6(a) and 6(b). Specifically, the SGs are positioned at the bottom of each vertical steel bar, 100 mm away from the wall foundation, to monitor the variations in strain distribution of the steel bars at the wall bottom cross-section in response to loading displacement. The wall's displacement measurement arrangement is illustrated in Fig. 6(c). The lateral deformation is directly measured by the linear variable differential transformer (LDVT) (D2) located at the top of the wall specimen. The slip of the bottom beam during wall loading is measured by the horizontal LDVT (D1). Additionally, two vertical LDVTs of D3 and D4 are utilized to survey the rigid rotation of the wall specimen. The wall lateral deformation is obtained by subtracting the deformation induced by the bottom beam slip and the deformation caused by the rigid rotation.

3 Test result

3.1 Failure process and mode

3.1.1 Crack propagation

As shown in Fig. 7, L-shaped wall has two faces. The lateral cyclic loading is along the symmetry axis of the L-shaped cross-section, so the force and deformation state of the two faces is the same, and they have similar crack

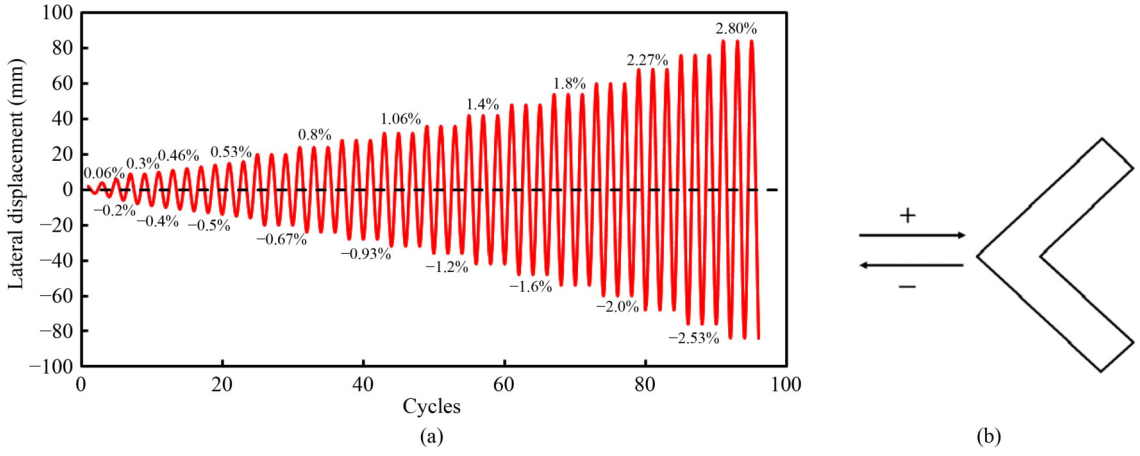

Fig. 5 Schematic diagram of lateral loading system: (a) lateral loading Schematic diagram; (b) positive and negative loading directions.

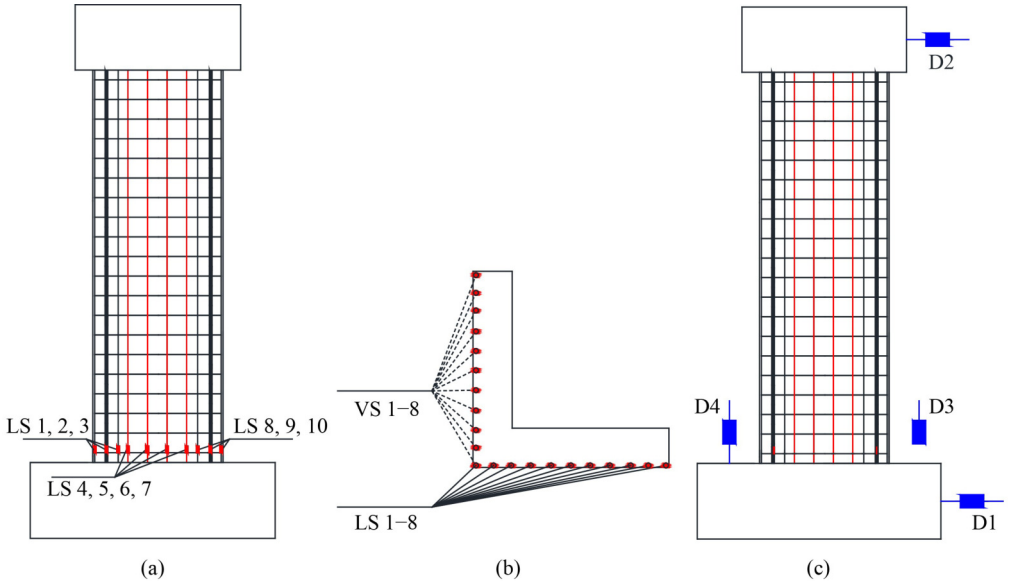

Fig. 6 Layout of SG and LDVTs of wall specimens: (a) elevation of strain gauge layout; (b) plane graph of strain gauge arrangement; (c) LVDTs.

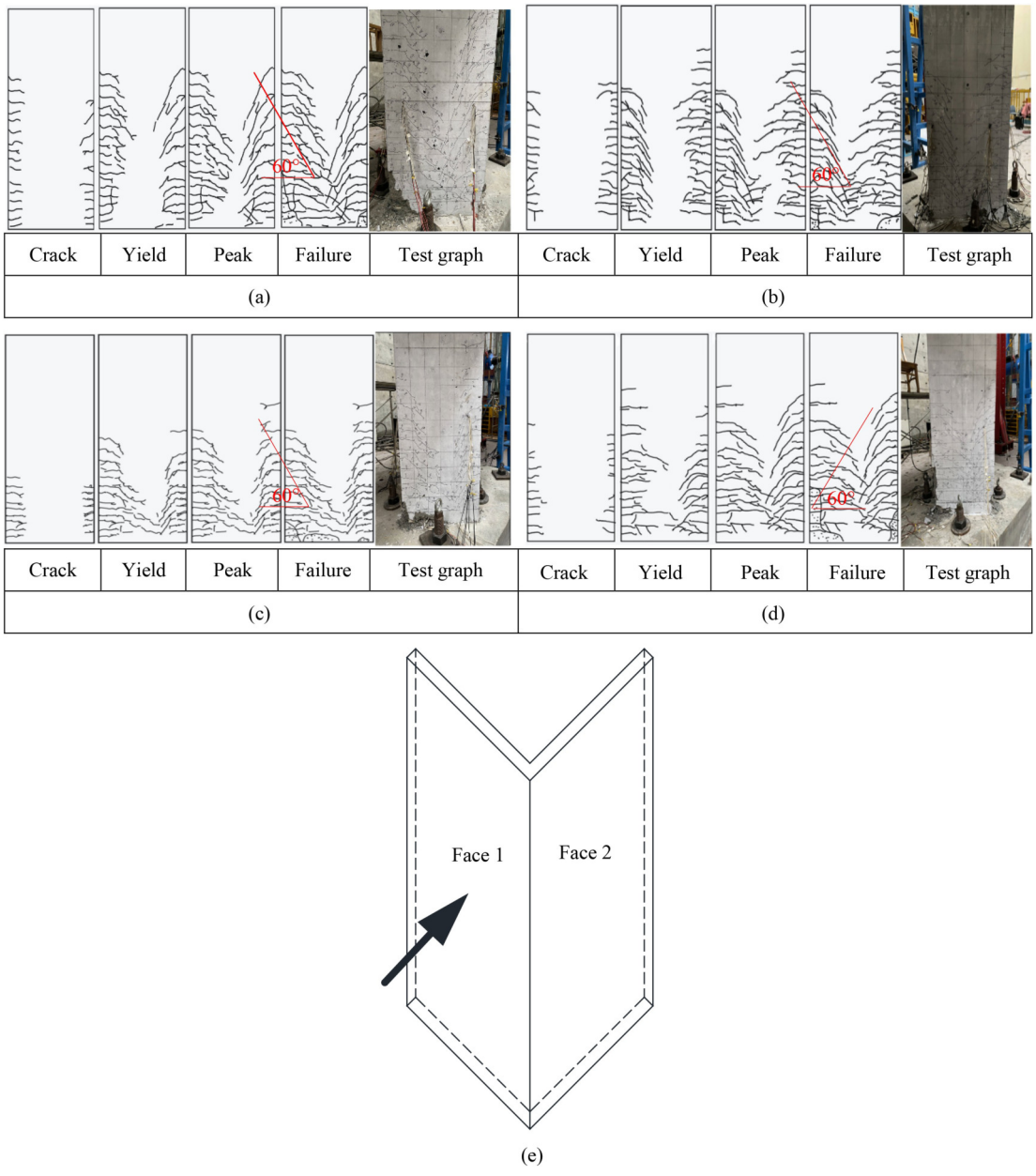

Fig. 7 Crack development: (a) C60-L; (b) C80-L; (c) (c) C60-S; (d) C80-S; (e) view direction

pattern. Therefore, we only present the crack development of Face 1. In the test, the crack propagation and failure modes of all four wall specimens were found to be similar, as detailed in Fig. 7, which shows the crack patterns of one flange face corresponding to crack, yield, peak, and failure points. Initially, horizontal short cracks emerged in the bottom tensile area of the wall under small displacements (drift ratio 0.33%–0.45%). As the loading displacement increased, more horizontal cracks emerged in the tensile area from specimen bottom to top (drift ratio 0.45%–1%). With the loading increase, the horizontal cracks close the wall edge progressively propagated downward and formed inclined cracks with the angle of approximately 60° (drift ratio 1%–1.5%). As the lateral loading displacement increased, the original cracks continued to propagate and crossed, and the concrete protective layer began to peel off. Finally, the shear wall failed owing to the large area crushing of the concrete in the bottom compression area (drift ratio 2.3%–3.7%). The angle of the inclined cracks is approximately 60°.

3.1.2 Failure analysis

Each shear wall specimen's failure modes and corresponding drift ratio is shown in Fig. 7. It can be observed that the failure modes are similar. Figures 8(a) and 8(b) respectively depict the front and side view angles of failure modes of Specimen C60-L. The concrete crushing degree at the corner of the LSRHCW specimen

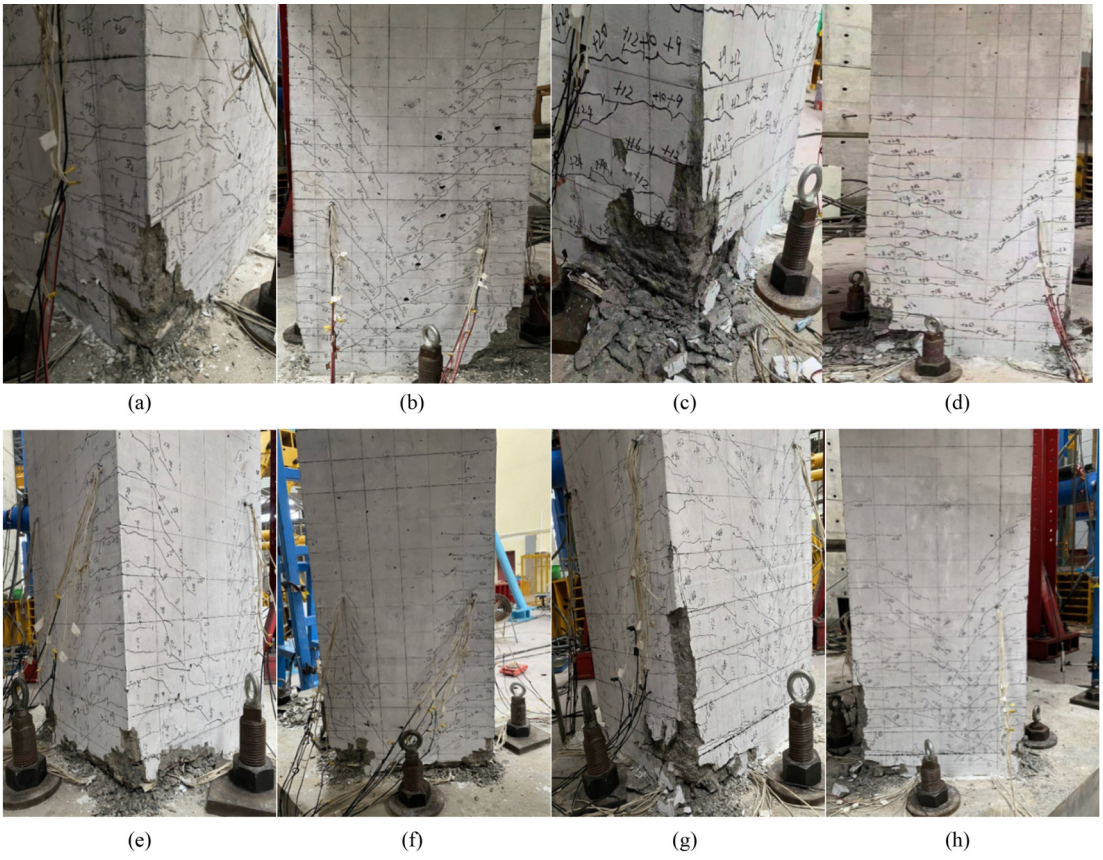

Fig. 8 Failure modes. (a) C60-L (3.03%); (b) C60-L (3.03%); (c) C80-L (3.03%); (d) C80-L (3.03%); (e) C60-S (2.45%); (f) C60-S (2.45%); (g) C80-S (2.38%); (h) C80-S (2.38%).

is higher than that at the free end, and no tensile fracture of steel bars is observed. The damaged wall specimens have many inclined cracks caused by the shear force, and the concrete at the toes crushed mainly caused by the bending moment, so the failure mode of the wall specimens belongs to flexure-shear mode. The failure of the wall specimens is owing to a slow strength decrease caused by the concrete crushing, and no reinforcing bars and shape steel fracture occurred, so the failure belongs to ductile mode. Figures 8(c) and 8(d) are failure mode diagrams of Specimen C80-L, where the concrete at the corner and the free ends is severely crushed. Compared with Specimen C60-L, the degree of concrete crushing is more severe, mainly because the ductility of C80 is lower than that of C60, moreover, the axial loading force of Specimen C80-L is higher. Figures 7(e) and 7(f) are failure modes of Specimen C60-S, and Figs. 8(g) and 8(h) are failure modes of Specimen C80-S, which have the same failure mechanism as the above shear wall specimens. In summary, increasing the strength of HSC (C60–C80) and decreasing the steel ratio (−55.6%) have no negative effect on the failure characteristics of the LSRHCW specimens.

Due to the fact that the loading direction of the lateral cyclic force on the L-shaped shear wall specimens was at a 45° angle to the length direction of the wall limbs, extensive concrete crushing occurred at both the bottom corner of the wall and the free end of the wall limb. In the existing cyclic loading tests on L-shaped shear wall specimens, the loading direction of the lateral cyclic force was often parallel to the length direction of one wall limb of the L-shaped shear wall specimen (unidirectional cyclic loading). This led to severe concrete crushing at the bottom of the wall limb parallel to the loading direction of the L-shaped shear wall, while the other wall limb (similar to the flange) only cracked and no concrete crushing occurred, as shown in Fig. 9. Therefore, it can be known that the failure modes of the L-shaped shear wall are completely different under different loading directions.

3.2 Hysteretic curves

Figure 10 shows the hysteretic curves of the above shear wall specimens. It shows that the hysteretic curves of each specimen are full, which indicates that the walls have excellent energy dissipation performance under high axial compression ratio of 0.5. The loading direction of the shear wall specimen forms an angle of 45° with the two limbs' length direction, and it leads to the obvious asymmetry of the hysteretic curves in both the positive and negative (±) loading directions. Some common

characteristics of the hysteretic curves can be obtained: The LSRHCW specimen kept elastic during the initial loading phase, and exhibited linear lateral force–displacement relationship. The area enclosed by the hysteretic curves was small, the residual deformation and the energy consumption were also very small. With the increase of loading displacements, the longitudinal reinforcement and shape steel yielded, concrete cracked, the area surrounded by the hysteretic curves gradually became full, and the stiffness degradation gradually became severe. In the same displacement target, the maximum force values corresponding to the second and third cyclic displacements were lower than that of the first cycle, which shows that the strength of the specimen is degraded under cyclic loading. Meanwhile, it can be also found that the hysteretic curve loops of the wall specimens equipped built with C60 and C80 concrete were full, and exhibited a small pinch effect. The hysteresis curves presented a gentle strength decline after the peak point. After the concrete was crushed, the strength decreased significantly until it dropped to 85% of the peak force and entered the failure stage. In general, the walls equipped with C60 and C80 concrete exhibit full hysteresis curve, long yield platform branch, good deformation performance, gentle strength decline, and achieve good safety performance.

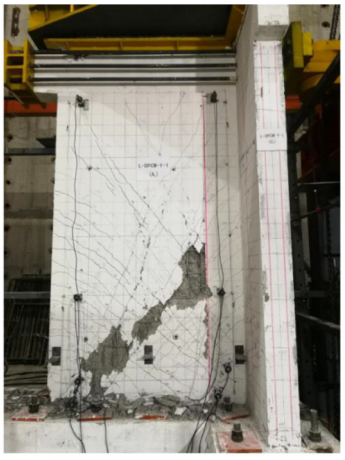

Fig. 9 Failure mode diagram of L-shaped shear wall specimen under unidirectional cyclic loading [45].

The force analysis of the L-shaped shear wall is carried out, as shown in Fig. 11, and it can be seen that the lateral load can be equal into two component forces along the length directions of the L-shaped wall limbs, which is equivalent to the force model of the two L-shaped shear walls (Figs. 11(a) and 11(b)). In the case of positive

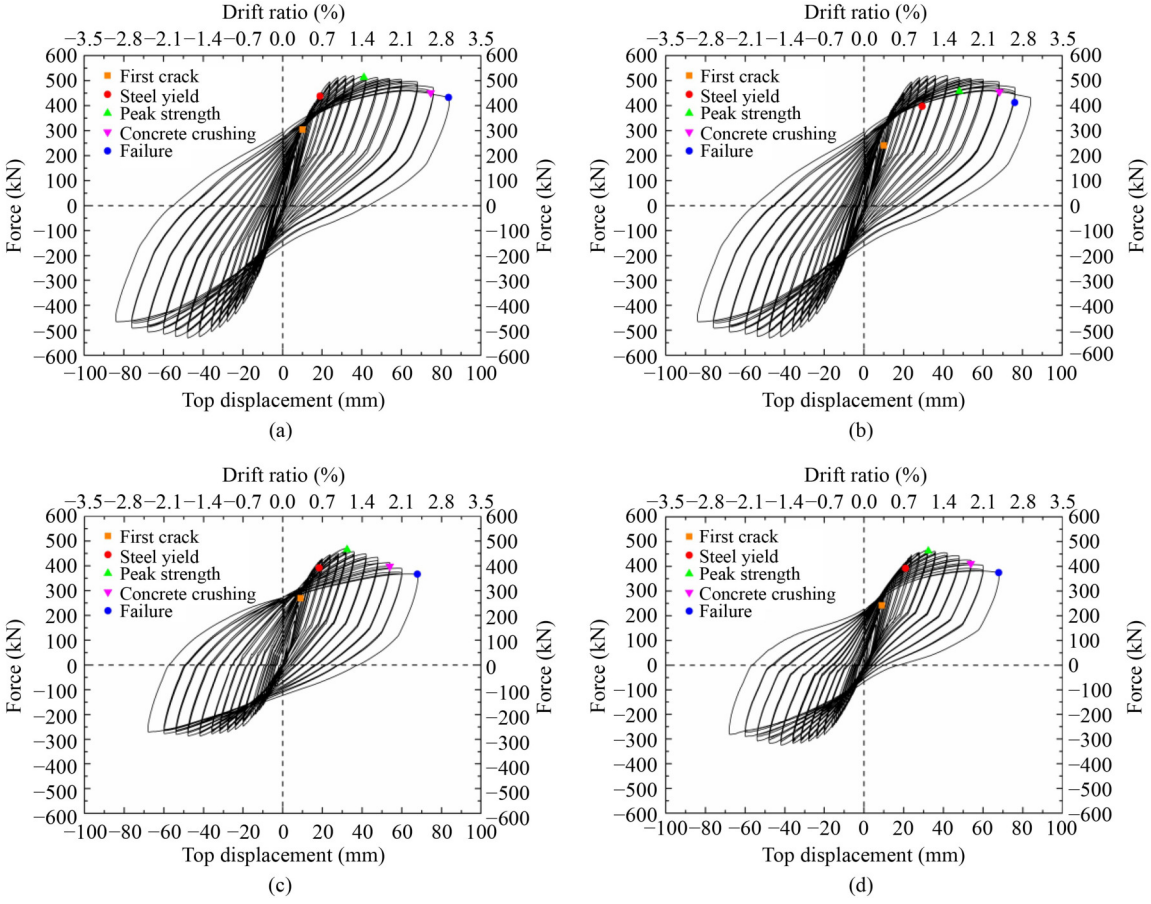

Fig. 10 Hysteresis curves: (a) C60-L; (b) C80-L; (c) C60-S; (d) C80-S.

loading, as shown in Fig. 11(a), the simplified equivalent Model 1: one limb of L-shaped shear walls is under full tension and the other limb under is under compression at the free end. For the negative loading, as shown in Fig. 11(b), the equivalent Model 2 is the opposite, one limb of the L-shaped shear wall is compressed, and the free end of the other leg is under tension. According to the experimental study of L-shaped shear walls [37], when the lateral load is loaded along the length direction of the wall limb, the bearing capacity is larger because the flange has more vertical steel bars in tension (Model 1). Therefore, it can be seen that the asymmetry of cross-section causes the asymmetry of hysteresis curves of L-shaped shear wall. When the load is positive loading, the load of the wall is larger, and the energy dissipation and stiffness are also larger.

The comparison of hysteretic curves of LSRHCW specimens with different strength concrete was shown in Fig. 12, and it is evident that the wall specimens with

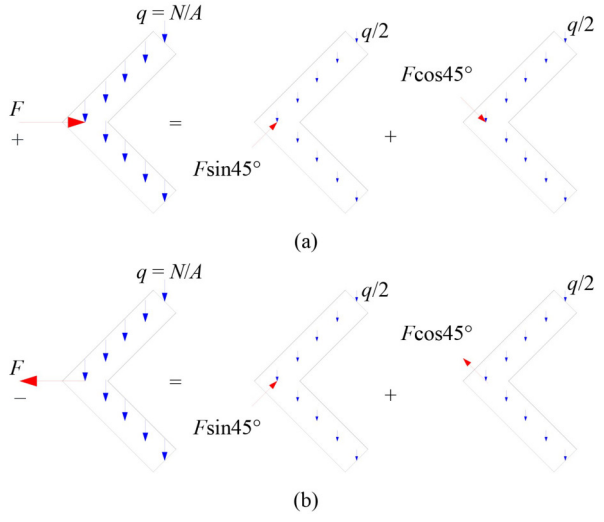

Fig. 11 Force analysis: (a) positive loading direction; (b) negative loading direction.

different concrete strength (from C60 to C80) have the similar hysteretic curves. This means that improving the concrete strength can help reduce the steel and reinforcement ratios and save the amount of shape steel required. The two specimens have similar loading/unloading stiffness, and their hysteretic curves presented a similar pinching effect. It can be also found that under each stage of loading displacement, the hysteretic loop area of the C60 specimens was larger compared with that of the C80 specimens, mainly because the C60 and C80 specimens are of equal strength design. Although the concrete strength of the C80 specimen is higher, its reinforcement ratio is reduced, resulting in lower energy consumption than that of the C60 specimen. The two specimens had the same drift ratio capacities, which shows good deformation performance. Therefore, improving the concrete strength of the wall can be an effective way to reduce the shape steel and reinforcement ratios of the LSRHCW while ensuring its hysteretic performance in this test.

For an L-shaped shear wall with unidirectional loading, that is, the loading direction of the lateral cyclic force is parallel to one of the limbs of the L-shaped shear wall, its hysteretic curves show a large asymmetry in the positive and negative loading directions. When the flange (wall limb perpendicular to the loading direction of the lateral) is in tension, the strength of the wall is larger, but the deformation capacity is relatively smaller. The hysteresis curves of L-shaped shear wall specimens under multi-direction loading are quite different from those in this paper.

3.3 Backbone curves

Figure 13 is the backbone curve comparison diagram of the above L-shaped shear wall specimen. The backbone curve of the wall specimens equipped with C60 and C80 can be roughly divided into linear, plastic, yield and falling branches. The initial branch is linear, and two

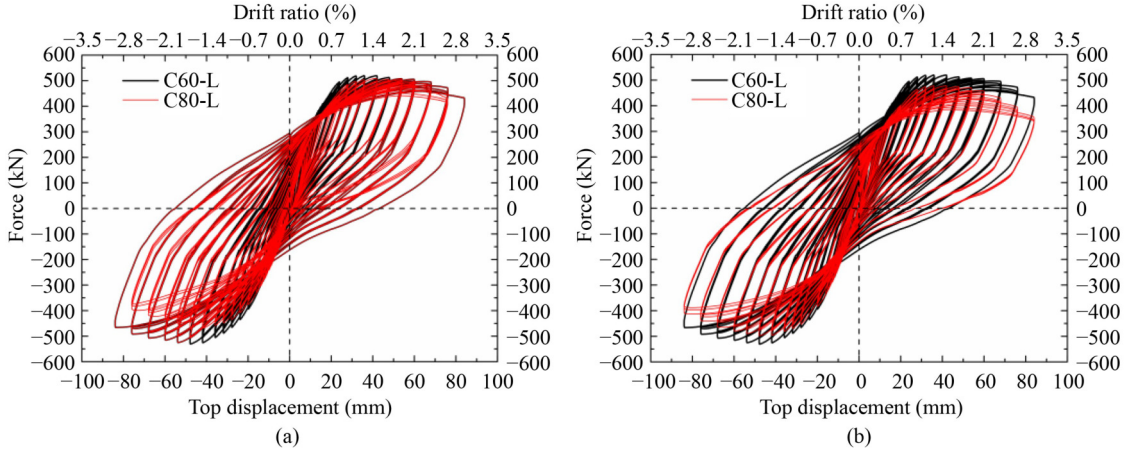

Fig. 12 Influence of concrete strength on hysteretic behavior of wall: (a) C60/80-L; (b) C60/80-S.

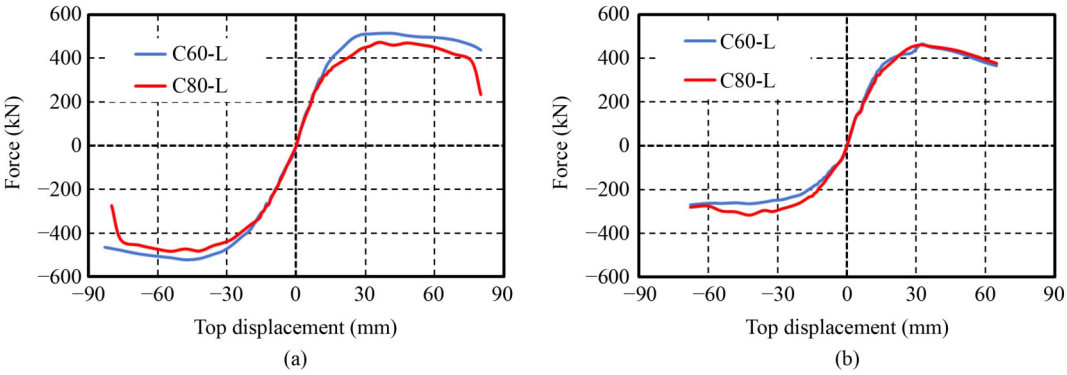

Fig. 13 Backbone curves: (a) C60/80-L; (b) C60/80-S

kinds of shear walls with different strength concrete have similar initial stiffness in positive and negative loading directions. With the yield and damage of the material, the backbone curves gradually enter the plastic branch. After the positive peak points, the bearing capacity of the specimen begins to decrease gradually until it fails. In the negative loading, the wall experienced a relatively obvious yield platform, and then, the bearing capacity decreased significantly. In the falling branch the bearing capacity of the wall decreased uniformly, showing good ductility.

4 Discussion

4.1 Strength and deformation analysis

Table 7 summarizes the characteristic values of the load–displacement curves for each shear wall specimen, including cracking, peak, yield, and ultimate points. The yield force and displacement are obtained using the method presented by Park [46] in Fig. 14. Due to the cross-section asymmetry, there is a noticeable difference between the load and displacement values of each characteristic point in the ± loading directions.

As a result of the large axial force on each specimen, the first crack appeared at a large drift ratio (≥ 0.40%). Compared to Specimen C60-S, the average load values at the cracking, yield, peak points of Specimen C80-S increased by −1.1%, 6.4%, and 6.3%, respectively. Compared to Specimen C60-L, the average load values at the cracking, yield, peak points of Specimen C80-L decreased by 0.4%, 7.1%, and 7.6%, respectively. Therefore, it can be concluded that the wall specimens have similar characteristic values of the load–displacement curve, and these results also indicate that replacing C60 concrete with HSC C80 can effectually decrease the steel and reinforcing bar ratios and has no significant impact on the average strength of LSRHCWs.

The force values of the wall specimens under positive and negative loading displacement is somewhat different due to the cross-section's asymmetry. When evaluating the bearing capacity, the smaller value of the peak force under ± loading direction should be taken as the strength

Table 7 Characteristic point value of load–displacement curve of each specimen

Specimen	Loading direction	Cracking point		Yield point		Peak point		θ_u (%)	u
		F_{cr} (kN)	θ_{cr} (%)	F_y (kN)	θ_y (%)	F_p (kN)	θ_p (%)		
C60-L	+	304.3	0.50	438.0	0.85	512.6	1.82	2.94	3.46
	–	–221.0	0.40	–435.9	1.16	–525.4	2.13	3.15	2.69
	Mean	262.6	0.45	437.0	1.00	519.0	2.00	3.03	3.03
C80-L	+	240.9	0.40	397.5	1.30	457.4	2.13	3.03	2.33
	v	–279.4	0.40	–428.4	0.95	–506.5	2.22	3.03	3.19
	Mean	260.1	0.40	413.0	1.12	481.9	2.18	3.03	2.71
C60-S	+	269.5	0.44	391.9	0.89	465.2	1.59	2.45	2.74
	–	–148.1	0.33	–237.8	1.20	–263.3	2.04	2.45	2.03
	Mean	208.8	0.39	314.8	1.05	364.3	1.82	2.45	2.32
C80-S	+	242.2	0.33	392.1	1.02	461.8	1.59	2.38	2.33
	–	–166.4	0.33	–277.7	1.15	–318.6	2.04	2.44	2.12
	Mean	204.3	0.33	334.9	1.09	390.2	1.82	2.44	2.24

of the wall specimens. Therefore, the strength of the specimen C60-L is 512.6 kN, and that of specimen C80-L is 457.4 kN. The strength of specimen C60-S is 263.3 kN, and that of specimen C80-S is 318.6 kN. For L-shaped long shear walls, increasing concrete strength and reducing the steel ratio will slightly reduce the walls' strength.

Ductility is an important factor that reflects the ability of the walls to stand up to earthquake action. Drift ratio capacity and ductility ratio are used to evaluate the walls' ductility performance. The ductility ratio is calculated using the following formula:

$$u = \frac{\Delta_u}{\Delta_y}. \tag{3}$$

Table 7 lists the ductility details of each wall specimen. The wall specimens exhibited different ductility ratios under positive and negative loading directions, with larger ductility observed under negative loading. The ductility ratio of each wall specimen ranged between 2.44 and 3.03. Specimen C60-L had a slightly larger ductility ratio than Specimen C80-L, while the ductility ratio of Specimen C60-S is similar to that of Specimen C80-S. These findings suggest that enhancing the concrete strength and reducing the shape steel and reinforcing bar ratios has slight influence on the ductility ratio of the LSRHCWs.

4.2 Stiffness degradation (SD) curve

The structural member's stiffness is closely tied to its shear force distribution within the structure, and the SD rate plays a crucial role in ensuring structural safety. To describe the SD characteristics of each wall specimen, the stiffness is measured using the secant stiffness of the peak load points during the first cycle at all loading displacement targets. The secant stiffness is calculated using

$$K_i = \frac{|+F_i| + |-F_i|}{|+X_i| + |-X_i|}, \tag{4}$$

where $+F_i$, $-F_i$ are respectively the ± peak forces of the wall specimen under ith loading displacement, and $+X_i$, $-X_i$ is the corresponding ± peak lateral displacement of the wall specimen. Figure 14(a) illustrates the s of L-shaped shear wall specimens with loading displacements. The graph reveals that the stiffness deteriorated rapidly during the initial stage and gradually in the later stage, similar to that of normal strength concrete shear walls. Specimen C80-L has an initial stiffness similar to that of C60-L shear wall. The corresponding stiffness of all four specimens is approximately 5.5 kN/mm at the ultimate point. Figure 15(a) shows the variation in SD rate of each specimen with the drift ratios, and it is apparent that the SD rate is nearly identical for all specimens.

In Fig. 15(b), the changes in secant stiffness of LSRHCW specimens with loading displacement are presented. The graph shows that the stiffness deteriorated quickly during the initial stage and gradually in the later stage. It is evident that the initial stiffness of specimen C80-S was similar to that of C60-S shear wall. The

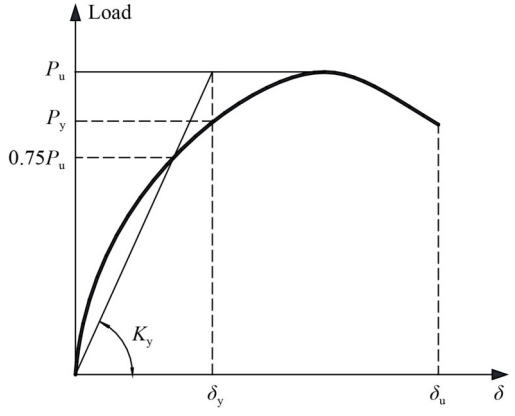

Fig. 14 Yield point definition method proposed by Park.

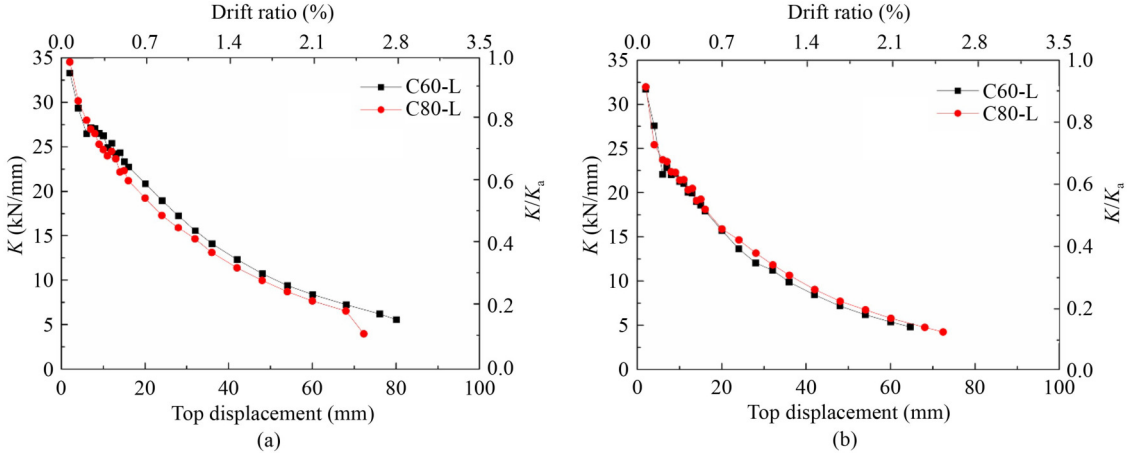

Fig. 15 SD curves: (a) L-shaped long shear wall specimens; (b) L-shaped short shear wall specimens.

corresponding stiffness of the two specimens was approximately 5 kN/mm at the ultimate point. Figure 14(b) displays the variation in SD rate of each specimen with the drift ratios, and it shows that the SD rates of each specimen are nearly identical.

4.3 Energy dissipation (ED) performance

During an earthquake, a shear wall member can help reduce the impact of the seismic action on the whole structures by dissipating energy using its nonlinear deformation and material damage. The cumulative ED E_{sum} and ED coefficient γ are analyzed to evaluate the ED performance of LSRHCW. E_{sum} and γ can be calculated by Eqs. (5) and (6), respectively.

$$E_{\text{sum}}^{n} = \sum_{i=1}^{n}\sum_{j=1}^{3} E_{ij}, \tag{5}$$

$$\gamma = \frac{S_{ABCDA}}{2\pi(s_{\Delta OBE} + s_{\Delta ODF})}, \tag{6}$$

where E_{ij} is the hysteresis loop area of the jth cycle of the ith loading target, S_{ABCDA} is the hysteresis loop area in Fig. 16, and $S_{\Delta OBE} + S_{\Delta ODF}$ is the area sum of ΔOBE and ΔODF.

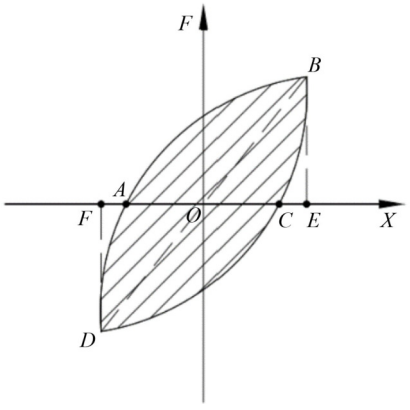

Fig. 16 Calculation diagram of γ.

Figure 17 shows the ED curves of each specimen. Figure 17(a) shows the cumulative ED of Specimen C60-L was higher than that of Specimen C80-L under different loading displacements, and the same trend is observed for Specimens C60/80-S with smaller dimensions. Therefore, it can be concluded that shear walls with low strength grade concrete have better energy dissipation performance. Although C80 concrete has higher strength than C60 concrete, it is brittle, less ductile, and has poor energy dissipation performance. Additionally, C60 concrete shear walls have higher steel ratios, which results in better ED performance compared to C80 concrete shear walls.

Figure 17(b) shows the γ variation of each specimen with the top displacement. The γ of each specimen were large, with a maximum value of 0.33, which is much higher than that of ordinary reinforced concrete shear walls (0.2). This indicates that the ED performance of the studied walls is good. The high γ is mainly due to the large shear-span ratio of the wall specimens, leading to a flexure-dominated failure mode, as well as the use of shape steel in the section, which greatly improves the SD performance of the walls. Additionally, it is found that the γ of C60 concrete shear walls is higher than that of C80 concrete shear walls, and the γ of shear walls with smaller sections is higher than that of shear walls with larger cross-sections, indicating that walls with smaller sections have better energy dissipation performance.

4.4 Strain analysis

The strain of shape steel and reinforcement bars is an indicator to evaluate the behavior of concrete shear walls under seismic loading. Figure 17 presents the locations of SG, and the height to the foundation of the wall specimens is 100 mm, shown as Fig. 5. The strain of shape steel and longitudinal reinforcement of the specimen C80-L have a similar variation trend with the

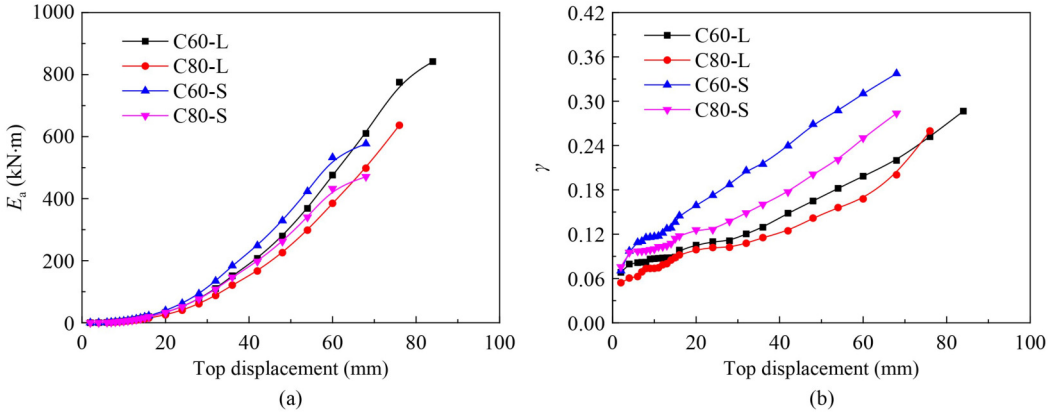

Fig. 17 Energy dissipation: (a) ED curves; (b) γ curves.

loading displacement. The strain change of the shape steel in cross-section corner in Fig. 18(a) shows that the shape steel entered compressive yield first due to the large axial force borne by the specimen. After the yield, the stress–strain curve became nonlinear, and the envelope area gradually increased. The strain changes of shape steel at both free ends in Figs. 18(b) and 18(c) have the same characteristics as the strain changes of the shape steel in cross-section corner, and they also entered the tension and compression yield state during the whole loading process. The strain changes of longitudinal bars at the corner are shown in Fig. 18(d), indicating that the longitudinal bars at the corner entered the tensile yield state when the loading displacement is 21.2 mm (0.94%). The longitudinal bars also entered the yield state before the wall specimens entered the ultimate bearing capacity state. The good cooperative working performance of section steel, HSC and longitudinal reinforcement can be used to effectively improve the bearing capacity of the shear walls under seismic loading.

5 Engineering application suggestion

According to the above cyclic loading test results of LSRHCWs, the following engineering application suggestions can be obtained.

1) LSRHCWs have high bearing capacity, energy dissipation and ductility performance under high axial compression ratio of 0.5, so it is suitable for tall and

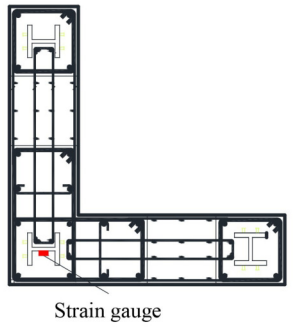

(a)

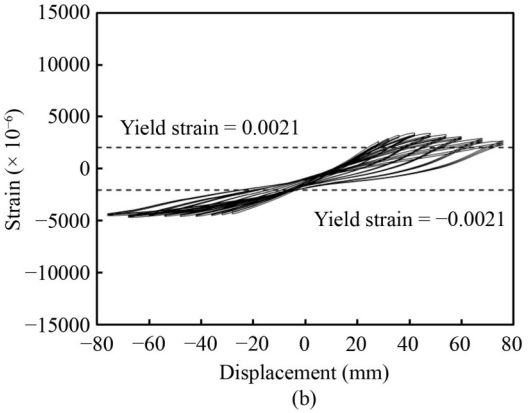

(b)

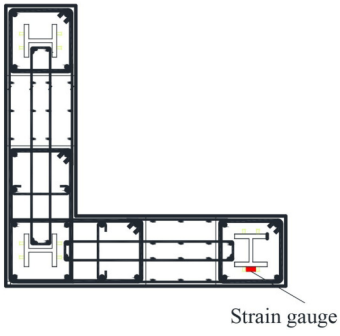

(c)

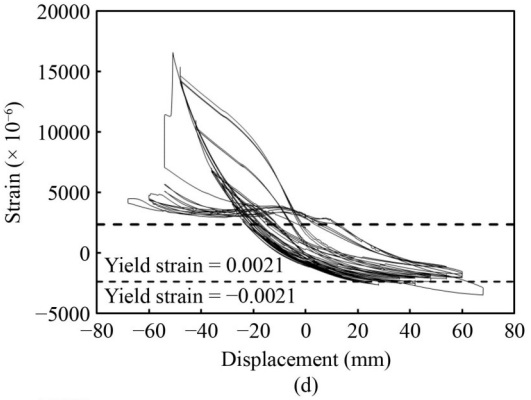

(d)

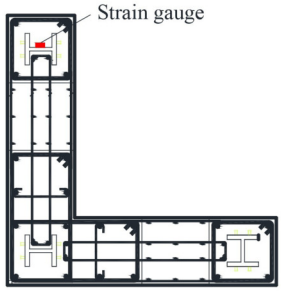

(e)

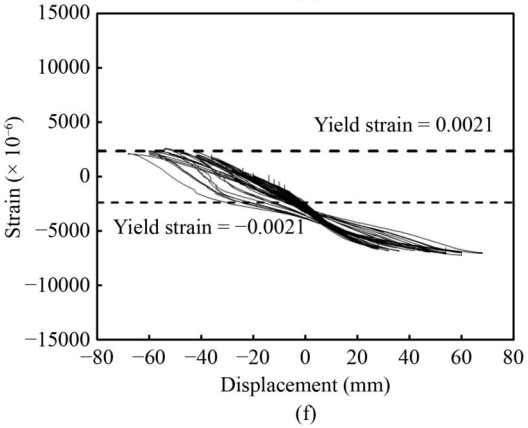

(f)

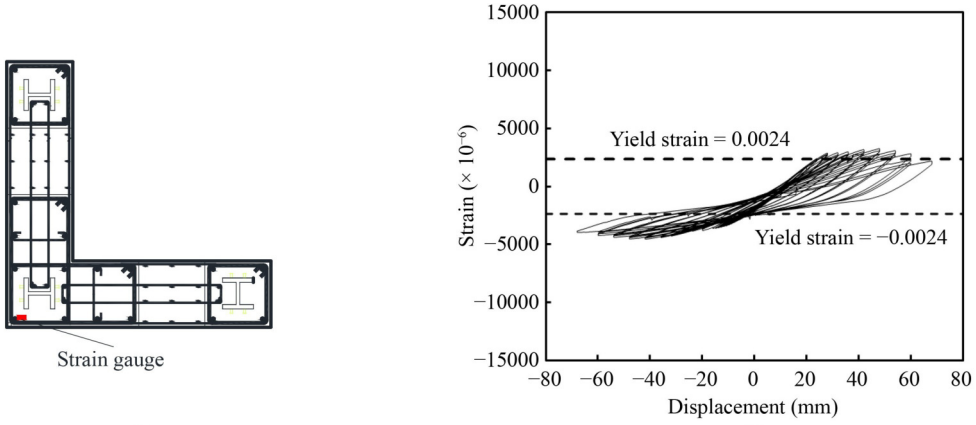

(g) (h)

Fig. 18 Strain change of shape steel and longitudinal reinforcement of specimen C80-L: (a) strain gauge location; (b) shape steel in cross-section corner; (c) strain gauge location; (d) shape steel in one free end; (e) strain gauge location; (f) shaped steel in the other end; (g) strain gauge location; (h) longitudinal bar in one free end

super-tall building structures. The shape steel and reinforcing bar ratios of LSRHCWs can be reduced by increasing the concrete strength, and it has a negligible influence on the seismic performance of LSRHCWs.

2) In the relevant literatures reporting L-shaped shear wall specimens loaded in the flange length direction, only the concrete at the free end of one wall limb is crushed, while the other wall limb remains intact. When LSRHCW specimens is loaded at 45°, the corner concrete damage is more serious, and the free end of the two limbs also has a large area of concrete crushing with no steel bar fracture. Therefore, attention should be paid to strengthening the corners and free ends of LSRHCWs.

3) HSC has greater brittleness and its ductility should be improved when used in shear walls at the bottom of tall and super-tall buildings. According to the results of the above test, integration of HSC with shape steel is a reasonable measure to enhance the ductility of HSC members.

6 Conclusions

This study investigated the seismic performance of LSRHCWs under high axial compression ratio of 0.5 using cyclic loading tests. The crack propagation, failure mechanism, hysteretic characteristics, strength, SD, deformation performance, energy dissipation performance, and steel strain of each wall specimen were studied, leading to the following conclusions.

1) All LSRHCW specimens failed in flexure-shear mode, which was owing to the strength decrease caused by concrete crushing. The extent of concrete crushing at the corner surpassed the degree witnessed at the free end. No tensile fracture and buckling of shape steel and reinforcing bars were observed.

2) The hysteretic curves of all tested wall specimens exhibit a full shape, indicating good energy dissipation performance under high axial compression ratios. Despite different concrete strengths and shape steel and reinforcing bar ratios, all shear wall specimens demonstrate comparable strength, stiffness, pinching effect, hysteresis loop envelope area, and drift ratio capacity. Therefore, enhancing the concrete strength can effectively lower the shape steel and reinforcing bar ratios, while maintaining a negligible impact on the hysteretic performance of the LSRHCWs.

3) The LSRHCW specimens have a large drift ratio from 2.4% to 3.03% under high axial loading ratios, which demonstrate excellent deformation performance. This result suggests that the shape steel can effectively enhance deformation capacity of HSC walls.

4) As the wall specimens reached the ultimate bearing capacity state, both the shape steel and longitudinal reinforcement had already entered the yield state. This indicates the good combined working performance of shape steel, longitudinal reinforcement, and HSC and their strength can be fully utilized.

5) LSRHCW specimens crafted with C80 concrete, coupled with lower ratios of shape steel and reinforcing bars, demonstrate a comparable performance in terms of bearing capacity, deformation resistance, initial stiffness, and deformation characteristics, as opposed to those constructed with C60 concrete and higher ratios of shape steel and reinforcing bars. This indicates that, under equivalent seismic resistance conditions, the amount of shape steel and reinforcing bar in LSRHCWs can be effectively reduced by increasing the strength grade of concrete.

Acknowledgements This work was supported by the National Key Research and Development Program of China (No. 2020YFB190140201).

Competing interests The authors declare that they have no competing interest.

References

1. Lu X, Zhang Y, Zhang H, Zhang H, Xiao R. Experimental study on seismic performance of steel fiber reinforced high strength concrete composite shear walls with different steel fiber volume fractions. Engineering Structures, 2018, 171: 247–259
2. Ni X, Cao S, Liang S, Li Y, Liu Y. High-strength bar reinforced concrete walls: Cyclic loading test and strength prediction. Engineering Structures, 2019, 198: 109508
3. Ni X, Lu N. Cyclic tests on T-shaped concrete walls built with high-strength reinforcement. Journal of Earthquake Engineering, 2021, 11: 1–26
4. Zhang J, Liu J, Li X, Cao W. Seismic behavior of steel fiber-reinforced high-strength concrete mid-rise shear walls with high-strength steel rebar. Journal of Building Engineering, 2021, 42: 102462
5. Zhou J, Fang X, Yao Z. Mechanical behavior of a steel tube-confined high-strength concrete shear wall under combined tensile and shear loading. Engineering Structures, 2018, 171: 673–685
6. Zhang H, Zhang Y, Lu X, Duan Y, Zhang H. Influence of axial load ratio on the seismic behavior of steel fiber-reinforced concrete composite shear walls. Journal of Structural Engineering, 2020, 146(1): 04019171
7. Nie J, Hu H, Fan J, Tao M, Li S, Liu F. Experimental study on seismic behavior of high-strength concrete filled double-steel-plate composite walls. Journal of Constructional Steel Research, 2013, 88: 206–219
8. Wu Y, Tang H, Lin X, Li L. Experimental study on seismic behaviour of high strength concrete shear walls with embedded cold-formed and thin-walled steel truss. Journal of Building Structures, 2014, 35(11): 44–52 (in Chinese)
9. Xu G, Guo T, Li A. Seismic resilient shear wall structures: A state-of-the-art review. Science China. Technological Sciences, 2023, 66(6): 1640–1661
10. Dong Y, Lu X. Overview of bond-slip research on steel reinforced concrete structures. Structural Engineering, 2005, 21(3): 82–87
11. Jiang D, Xiao C, Chen T. Experimental study of the compression-bending behavior of high-strength concrete steel composite shear walls. China Civil Engineering Journal, 2012, 45(3): 17–25 (in Chinese)
12. Chen T, Xiao C, Tian C. Experimental study of the compression-bending behavior of composite shear walls of high axial compression ratios. China Civil Engineering Journal, 2011, 44(6): 1–7 (in Chinese)
13. Xu G, Li A. Seismic performance of a new type precast concrete sandwich wall based on experimental and numerical investigation. Soil Dynamics and Earthquake Engineering, 2019, 122: 116–131
14. Massone L M, Sayre B L, Wallace J W. Load−deformation responses of slender structural steel reinforced concrete walls. Engineering Structures, 2017, 140: 77–88
15. Soon H C, Bryce T, William D C. Structural steel boundary elements for ductile concrete walls. Journal of Structural Engineering, 2004, 130(5): 763–768
16. Dong Y, Lu X, Ding Z. Calculation method for shear resistant capacity of steel reinforced concrete walls. Engineering Mechanics, 2007, 24: 114–118 (in Chinese)
17. Huang X, Zhao S. Experimental study on low shear wall with reinforced concrete frame. Journal of Southwest Jiaotong University, 1999, 31(5): 535–539
18. Liang X, Bai L, Yang H. Experimental study on the seismic behaviour of high performance steel−concrete shear walls. Engineering Mechanics, 2010, 27(10): 131–138 (in Chinese)
19. Luo Y, Zhao S. The experimental investigation of antiseismic behaviour on the SRC framed squat shear wall. Journal of Xi'an Highway University, 1999, 19(2): 66–69 (in Chinese)
20. Fang M, Li G, Li Y. Seismic behavior of steel reinforced concrete mid-rise shear wall. Journal of Shenzhen University Science and Engineering, 2012, 29(1): 38–44
21. Wei Y, Qian J, Zhao Z. Lateral loading experiment of SRC low shear walls with high axial force ratio. Industrial Construction, 2007, 37(6): 76–79 (in Chinese)
22. Qiao Y,Qian J, Fang E. Experimental study on shear behavior of steel reinforced concrete shear wall. Journal of building structure, 1995(8): 3–7
23. Sun J,Xu P, Xiao C. Experimental study on shear behaviour of concrete wall with difference types of reinforcement. Journal of Building Structure, 2008, 38(6): 6–10
24. Wang Z, Fang E, Qian J. Bending properties of steel bone concrete shear wall. Building Structure, 1998, (2): 13–16 (in Chinese)
25. Ji X, Sun Y, Qian J, Lu X. Seismic behavior and modeling of steel reinforced concrete (SRC) walls. Earthquake Engineering & Structural Dynamics, 2015, 44(6): 955–972
26. Lu X, Yang J. Seismic behavior of T-shape steel reinforced concrete shear walls in tall buildings under cyclic loading. Structural Design of Tall and Special Buildings, 2015, 24(2): 141–157
27. Dan D, Fabian A, Stoian V. Nonlinear behavior of composite shear walls with vertical steel encased profiles. Engineering Structures, 2011, 33(10): 2794–2804
28. Bai L, Zhou T, Liang X. Study on the performance design method of steel high strength concrete shear walls. China Civil Engineering Journal, 2014, 47(5): 9–17 (in Chinese)
29. Hoult R, Doneux C, Pacheco de Almeida J. Tests on reinforced concrete U-shaped walls subjected to torsion and flexure. Earthquake Spectra, 2023, 39(4): 2685–2710
30. Hoult R D. Shear lag effects in reinforced concrete c-shaped walls. Journal of Structural Engineering, 2019, 145(3): 04018270
31. Menegon S J, Wilson J L, Lam N T K, Gad E F. Experimental assessment of the ultimate performance and lateral drift behaviour of precast concrete building cores. Advances in Structural Engineering, 2020, 23(12): 2597–2613
32. Ma J, Zhang Z, Li B. Experimental assessment of T-shaped reinforced concrete squat walls. ACI Structural Journal, 2018, 115(3): 621–634
33. Eom T S, Nam H S, Kang S M. Biaxial interaction and load contour method of reinforced concrete T-shaped structural walls. ACI Structural Journal, 2018, 115(1): 151–161
34. Zhang Z, Li B. Seismic performance assessment of slender T-shaped reinforced concrete walls. Journal of Earthquake Engineering, 2016, 20(8): 1342–1369
35. Lan W, Zhang Z, Li B. Seismic performance of T-shaped steel-

concrete composite structural walls subjected to loadings from different directions. Journal of Constructional Steel Research, 2017, 128: 7–18

36. Lim W Y, Kang T H K, Hong S G. Cyclic lateral testing of precast concrete T-walls in fast low-rise construction. ACI Structural Journal, 2016, 113(1): 179–189
37. Karamlou A, Kabir M Z. Experimental study of L-shaped slender R-ICF shear walls under cyclic lateral loading. Engineering Structures, 2012, 36: 134–146
38. Chaouch A A, Boutemeur R, Bechtoula H, Bali A. Numerical study on shear stress variation of RC wall with l shaped section. Periodica Polytechnica. Civil Engineering, 2015, 59(1): 15–25
39. Kabir M. Z, Vasheghani-Farahani R. Experimental investigation of performance in L-shaped wall to wall corner connections of 3D Panels subjected to lateral cyclic loading. Structural Engineering and Mechanics, 2009, 33(5): 649–652
40. JGJ3-2010. Technical Specification for Concrete Structures of Tall Building. Beijing: China Architecture & Building Press, 2016 (in Chinese)
41. GB 50010-2010. Code for Design of Concrete Structures. Beijing: China Architecture & Building Press, 2016 (in Chinese)
42. GB/T 50081-2002. Standard for Test Method of Mechanical Properties on Ordinary Concrete. Beijing: China Architecture & Building Press, 2003 (in Chinese)
43. GB/T 228.1-2010. Metallic Materials-tensile Testing-Part 1: Method of Test at Room Temperature. Beijing: Standards Press of China, 2011 (in Chinese)
44. JGJ/T 101-2015. Specification for Seismic Test of Buildings. Beijing: Ministry of Housing and Urban-Rural Development, 2015 (in Chinese)
45. Gu Q, Zhao D, Tan Y, Gao H, Deng Q, Wang X. Experimental study on L-shaped precast concrete superposed shear walls under quasi-static cyclic loading with different axial compressive load ratios. Engineering Structures, 2022, 254: 113857
46. Park R. Evaluation of ductility of structures and structural assemblages from laboratory testing. Bulletin of the New Zealand Society for Earthquake Engineering, 1989, 22(3): 155–166